Chemical Papers (2019) 73:1879–1891
https://doi.org/10.1007/s11696-019-00739-4

ORIGINAL PAPER

Conformational, structural, electronic, and vibrational investigations on 5-methyl-4-(2-thiazolylazo)resorcinol by FT-IR, FT–Raman, NMR, and DFT

Y. Erdogdu[1] · Ü. C. Başköse[2] · S. Sağlam[1]

Received: 1 November 2018 / Accepted: 6 March 2019 / Published online: 13 March 2019
© Institute of Chemistry, Slovak Academy of Sciences 2019

Abstract
The all conformers of 5-methyl-4-(2-thizolylazo)resorcinol have been identified by Spartan 13 software. All conformers have been optimized B3LYP/6-311G (d, p) level of theory in Gaussian 09 software. According to potential energy surface search, 5-methyl-4-(2-thizolylazo)resorcinol has eight conformers. All the structural parameters of the most stable conformer of 5-methyl-4-(2-thizolylazo)resorcinol are predicted using DFT (B3LYP) method with the same basis set given above. The vibrational frequencies are recorded by the Fourier transform infrared (FT-IR 4000–550 cm^{-1}) and Fourier transform Raman (FT–Raman; 4000–100 cm^{-1}) spectra in the powder form. The vibrational frequencies are predicted and compared with experimental FT-IR and FT–Raman ones. The experimental ^{1}H and ^{13}C NMR spectra have been recorded and compared with the theoretical chemical shifts determined by the GIAO method. The results of UV–Vis spectra of molecule are also presented. Theoretical results compared with the experimental results for the identification and characterization of 5-methyl-4-(2-thizolylazo)resorcinol molecule.

Keywords 5-Methyl-4-(2-thizolylazo)resorcinol · DFT · FT-IR and FT–Raman spectra · NMR and UV–Vis spectra

Introduction

Organic ligands such as 5-methyl-4-(2-thizolylazo)resorcinol (MTR) have been used in many experimental works up to now. Zaitoun et al. reported a study on the solid-phase extraction. It is a powerful separation method for sample preparation. In that study, MTR was used as a solid-phase extractant to remove zinc ions (Zaitoun et al. 2014a) and Cu(II) (Zaitoun et al. 2014b) in the water samples. The second one, determination of Co(II) ion as Co(II)/MTR was possible by means of reversed-phase high-performance liquid chromatography. In those works, any interference by universal metal ions could not be use (Chung and Chung 2003). Third from them, the effect of cetylpyridinium chloride (CPC) surfactant on the oxidation of MTR have examined using H_2O_2 (Menek et al. 2006). Fourth from them, simple and rapid co-precipitation procedure using nickel(II)-MTR precipitate has been proposed for gold(III), palladium(II), and lead(II) in environmental samples prior to their flame atomic absorption spectrometric determinations (Soylak and Tuzen 2008).

In analytical chemistry, the determination of metals ions is made using a heterocyclic azo reagent. Some of the simplest members of this class of reagents are compounds of the azo group such as 4-(2-thiazolilazo)resorcinol (TAR); 3-hydroxy-4-(1,3-thiazol-2-ylhydrazono)cyclohexa-2,5-dien-1-one; 2-(2, 4-(dihydroxyphenylazo) thiazole). This azo reagent can exist in three forms depending on the acidity in aqueous solutions. First of them is cationic form, which is protonated on the nitrogen atom in the compound. Second of them is molecular form. The last one is a form, which is ionized by hydroxyl groups of resorcinol ring (Smolinska et al. 2015).

In the spectrophotometric determination of platinum (Subrahmanyam and Eshwar 1976a) and transition (Gavazov et al. 2007; Gaokar and Eshwar 1982; Subrahmanyam and Eshwar 1976a, b) metals, TAR is the spectrophotometric reagent. TAR is a colored compound. In the visible portion of the spectrum, it has the absorbance maximum

✉ Y. Erdogdu
yusuferdogdu@gmail.com

[1] Department of Physics, Gazi University, Ankara, Turkey

[2] Photonics Application and Research Center, Gazi University, Ankara, Turkey

of its solution. Changing the existence form of the reagent is reflected by a significant shift (85 nm) of the maximum absorbance band to the long-wavelength range of the spectrum at the transition from protonated (cation) to molecular as well as dissociated forms. One-ionized azo reagents can exist in azo- or quinone hydrazo form, which is reflected in their reactivity.

The present work is detailed study of the structure, and spectroscopic and electronic properties of MTR molecule were unambiguously deduced by the experimental and theoretical methods. The DFT [B3LYP/6-311G(d,p)] calculations have been performed to study the molecular structure, and spectroscopic and electronic properties for MTR molecule. The electronic and spectroscopic properties of the studied compound have been predicted using the same level of theory.

Theoretical

Conformational distribution of MTR molecule was provided by scanning the potential energy surface Spartan 13 (Spartan 2008) program. To do this, Merck Molecular Force Field (MMFF) (Halgren 1996) method was used. After determining all conformations to identify the most stable conformation, geometry optimization was calculated with the Gaussian 09 (Frisch et al. 2009) program. Molecular geometries were fully optimized by the force gradient method using Berny's algorithm (Schlegel 1975) and the standard convergence criteria for geometry optimization. All the calculations are performed by the default convergence criteria without any constraint in the geometry. Furthermore, for the vibrational frequency and some electronic properties of MTR, molecule was carried out with Gaussian 09 program and GaussView 3.0 (Frisch et al. 2000) graphical interface. In all calculations such as geometry optimization, vibrational frequency and other molecular property calculations were performed by B3LYP (Becke 1988, 1993; Lee et al. 1988) functional and 6-311G(d,p) basis set. The vibrational assignments were made on the basis of the potential energy distribution (PED) determined with scaled quantum mechanics (SQM (2013)) program based on DFT calculation. Only PED components $\geq 10\%$ were evaluated to perform the final assignment. In addition, the Raman activities were converted to Raman intensities by means of RaInt program (Michalska 2003). NMR analysis has been done using Gauge independent atomic orbital (GIAO) method. The ^{1}H and ^{13}C NMR spectra calculations were performed by Gaussian 09 program package. In addition, the UV–Vis spectra, frontier molecular orbital analysis, and density-of-state analysis were performed.

Experimental

MTR molecule was supplied from Sigma-Aldrich [AL(37422-56-3)]. The FT-IR spectrum of MTR was recorded in the range of 4000–550 cm^{-1} (the spectral resolution was 4 cm^{-1} and 32 scans) with Bruker Vertex 80 FT-IR spectrometer equipped with a diamond crystal ATR (attenuated total reflectance) accessory. The Raman spectrum of sample was measured on a Bruker FRA106/S instrument operating at the 1064 nm exciting line of Nd:YAG laser (the spectral resolution was 4 cm^{-1} and 512 scans). UV–Vis absorption spectra of MTR were performed by Lambda 2S, Perkin Elmer UV–Vis spectrometer at RT in the range of 200–1100 nm. ^{1}H and ^{13}C NMR spectra were recorded on a Bruker Avance 300 MHz spectrometer in DMSO-d_6.

Results and discussion

Conformational analysis and structural properties

The conformational analysis shows that the free MTR molecule has eight conformers (see Figs. 1 and 2). In the geometry optimization, the input files were taken from the conformational analysis results. The obtained geometry was optimized by DFT/B3LYP method with the 6-311G(d,p) basis set. Minimizing the energies with respect to all the geometrical parameters without imposing any molecular symmetry constraints optimized the geometry predicted from conformational analysis. Consider the energy differences between the global minimum (lowest energy) conformer and the other seven conformers (see Table 1). According to the lowest energy conformer, the relative energy of the higher energy conformers was obtained at 3.806 kcal/mol, 4.236 kcal/mol, and 7.345 kcal/mol, respectively. The result of conformational analysis shows that conformer-1 is favorable than the other conformers at room temperature.

The optimized geometric parameters are given in Table 1 and Fig. 3. C_2–S and C_6–S bond distances were predicted about 1.73 Å and 1.77 Å, respectively. C–C bond distances of resorcinol ring (1.4 Å) were determined shorter than C–C bond distances of methyl group (1.5 Å) and longer than C–C bond distance of thizolylazo ring (1.3 Å). According to the structure of resorcinol, the benzene rings are regular plane hexagons, the distance between the carbon atoms being 1.39 Å. The centers of the hydroxyl groups (oxygen atoms) lie at 1.36 Å from the centers of the ring carbon atoms (Robertson 1936). The length of the methyl group bond to aromatic carbon

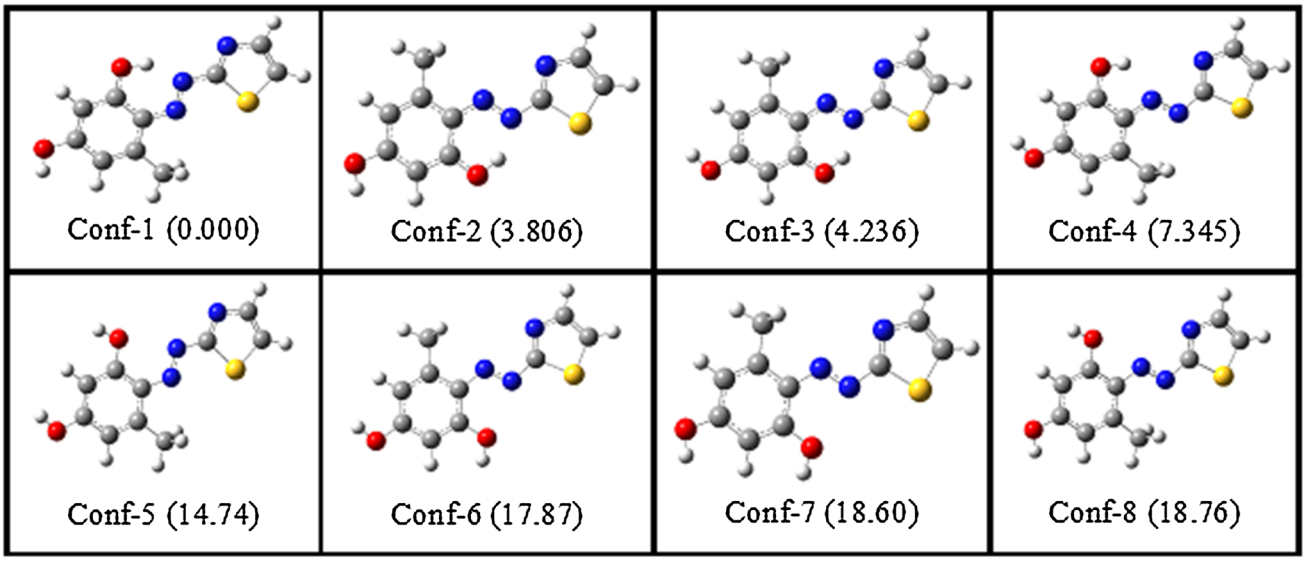


Fig. 1 Conformational analysis results of MTR molecule

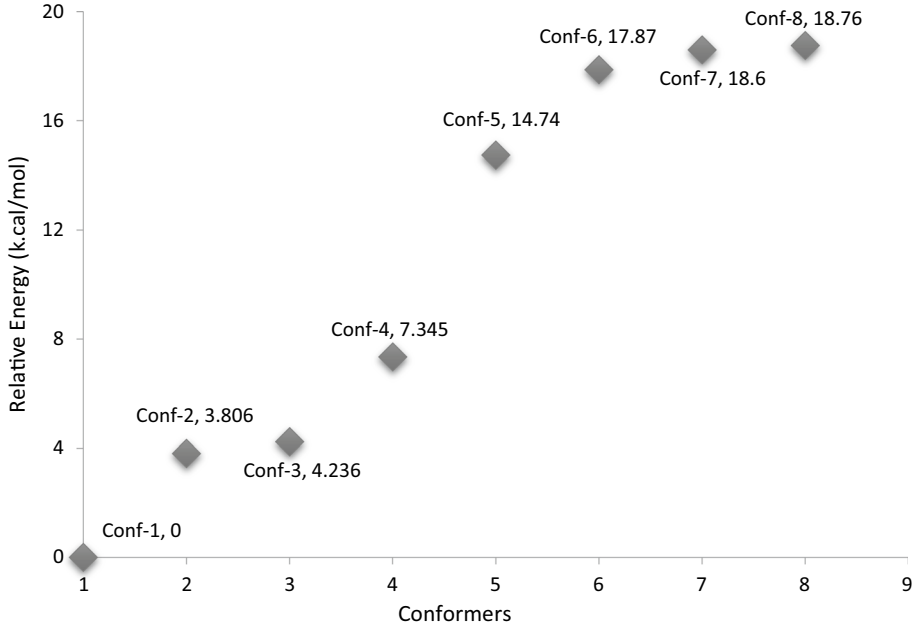


Fig. 2 The energy profile of the conformational analysis for MTR molecule

atoms is 1.53 Å (Brockway and Roberts 1939). All of the C–H, C–N, C–O, and O–H bonds of the optimized MTR molecule are equivalent between each other. N = N double-bond length was predicted about 1.27 Å by B3LYP/6-311 G(d,p) level of theory. According to calculated dihedral angles, structure of the MTR is planer geometry outside of H atoms of the methyl group. Bond angles were observed a symmetric geometry. Bond angle values changed between 106° and 128°. Due to the stable ring arrangement, only just thizolylazo ring's C_2–S_7–C_6 bond angle was observed on minimum value (87.65°) (Seferoğlu et al. 2009).

Vibrational analysis

The MTR molecule possesses Cs point group symmetry and has 25 atoms ($C_{10}H_9N_3O_2S$) with 69 normal modes. It consists of a thizolylazo ring and resorcinol ring, connected to each other with a chain (••N_8••N_9••). In addition, resorcinol ring has one methyl group and two OH group. All the vibrations are active in both IR and Raman spectra. The experimental Fourier Transform Infrared (FT-IR) and Fourier Transform–Raman (FT–Raman) spectra of MTR molecule are shown in Figs. 4 and 5. The

Table 1 Optimized geometric parameters of MTR

Bond lengths (Å)	DFT	X-ray	Bond angles (°)	DFT	X-ray	Dihedral angles (°)	DFT	X-ray
C_1–C_2	1.365	1.342[b]	C_2–C_1–H_3	124.8	122.0[b]	H_3–C_1–C_2–H_4	0.0	0.1[b]
C_1–H_3	1.082	0.930[b]	C_2–C_1–N_5	116.0	116.0[b]	H_3–C_1–C_2–S_7	180.0	179.9[b]
C_1–N_5	1.367	1.370[b]	H_3–C_1–N_5	119.1	122.1[b]	N_5–C_1–C_2–H_4	180.0	179.9[b]
C_2–H_4	1.079	0.930[b]	C_1–C_2–H_4	128.4		N_5–C_1–C_2–S_7	0.0	0.1[b]
C_2–S_7	1.733	1.720[b]	C_1–C_2–S_7	110.6	110.4[b]	C_2–C_1–N_5–C_6	0.0	0.2[b]
N_5–C_6	1.303	1.306[b]	H_4–C_2–S_7	120.9	124.8[b]	H_3–C_1–N_5–C_6	180.0	179.8[b]
C_6–S_7	1.775	1.733[b]	C_1–N_5–C_6	110.8	110.2[b]	C_1–C_2–S_7–C_6	0.0	0[b]
C_6–N_8	1.382	1.378[b]	N_5–C_6–S_7	114.9	114.9[b]	H_4–C_2–S_7–C_6	180.0	180[b]
N_8–N_9	1.275	1.300[b]	N_5–C_6–N_8	122.0	119.9[b]	C_1–N_5–C_6–S_7	0.0	0.1[b]
N_8–H_{20}	1.693		S_7–C_6–N_8	123.1	125.3[b]	C_1–N_5–C_6–N_8	180.0	178.4[b]
N_9–C_{10}	1.373	1.360[b]	C_2–S_7–C_6	87.6	88.5[b]	N_5–C_6–S_7–C_2	0.0	0.1[b]
C_{10}–C_{11}	1.437	1.392[a]	C_6–N_8–N_9	115.3	113.9[b]	N_8–C_6–S_7–C_2	180.0	178.4[b]
C_{10}–C_{12}	1.425	1.394[a]	N_8–N_9–C_{10}	117.3	117.3[b]	N_5–C_6–N_8–N_9	180.0	180
C_{11}–C_{13}	1.393	1.388[a]	N_9–C_{10}–C_{11}	124.2		S_7–C_6–N_8–N_9	0.0	1.5[b]
C_{11}–O_{19}	1.331	1.380[a]	N_9–C_{10}–C_{12}	116.4		C_6–N_8–N_9–C_{10}	180.0	179.2[b]
C_{12}–C_{14}	1.380	1.388[a]	C_{11}–C_{10}–C_{12}	119.4	118.4[a]	N_8–N_9–C_{10}–C_{11}	0.0	
C_{12}–C_{21}	1.507		C_{10}–C_{11}–C_{13}	120.0	121.4[a]	N_8–N_9–C_{10}–C_{12}	180.0	
C_{13}–C_{15}	1.387	1.388[a]	C_{10}–C_{11}–O_{19}	121.8	122.3[a]	N_9–C_{10}–C_{11}–C_{13}	180.0	
C_{13}–H_{16}	1.082	0.960[a]	C_{13}–C_{11}–O_{19}	118.2	116.3[a]	N_9–C_{10}–C_{11}–O_{19}	0.0	
C_{14}–C_{15}	1.409	1.374[a]	C_{10}–C_{12}–C_{14}	119.2	121.4[a]	C_{12}–C_{10}–C_{11}–C_{13}	0.0	0.8[a]
C_{14}–H_{17}	1.086	0.980[a]	C_{10}–C_{12}–C_{21}	120.3		C_{12}–C_{10}–C_{11}–O_{19}	180.0	179.8[a]
C_{15}–O_{18}	1.355	1.393[a]	C_{14}–C_{12}–C_{21}	120.4		N_9–C_{10}–C_{12}–C_{14}	180.0	
O_{18}–H_{25}	0.963	0.850[a]	C_{11}–C_{13}–C_{15}	119.5	119.0[a]	N_9–C_{10}–C_{12}–C_{21}	0.0	
O_{19}–H_{20}	0.994	0.870[a]	C_{11}–C_{13}–H_{16}	119.7	120.0[a]	C_{11}–C_{10}–C_{12}–C_{14}	0.0	0.7[a]
C_{21}–H_{22}	1.092		C_{15}–C_{13}–H_{16}	120.7	121.0[a]	C_{11}–C_{10}–C_{12}–C_{21}	180.0	
C_{21}–H_{23}	1.092		C_{12}–C_{14}–C_{15}	120.6	118.8[a]	C_{10}–C_{11}–C_{13}–C_{15}	0.0	0.3[a]
C_{21}–H_{24}	1.091		C_{12}–C_{14}–H_{17}	119.9	121.0[a]	C_{10}–C_{11}–C_{13}–H_{16}	180.0	179.0[a]
			C_{15}–C_{14}–H_{17}	119.4	121.0[a]	O_{19}–C_{11}–C_{13}–C_{15}	180.0	179.7[a]
			C_{13}–C_{15}–C_{14}	121.2	121.0[a]	O_{19}–C_{11}–C_{13}–H_{16}	0.0	2.0[a]
			C_{13}–C_{15}–O_{18}	117.3	116.9[a]	C_{10}–C_{11}–O_{19}–H_{20}	0.0	2.0[a]
			C_{14}–C_{15}–O_{18}	121.5	122.1[a]	C_{13}–C_{11}–O_{19}–H_{20}	180.0	178.0[a]
			C_{15}–O_{18}–H_{25}	109.6	111.0[a]	C_{10}–C_{12}–C_{14}–C_{15}	0.0	
			C_{11}–O_{19}–H_{20}	107.4		C_{10}–C_{12}–C_{14}–H_{17}	180.0	179.0[a]
			C_{12}–C_{21}–H_{22}	111.1		C_{21}–C_{12}–C_{14}–C_{15}	180.0	
			C_{12}–C_{21}–H_{23}	111.1		C_{21}–C_{12}–C_{14}–H_{17}	0.0	
			C_{12}–C_{21}–H_{24}	110.5		C_{10}–C_{12}–C_{21}–H_{22}	− 59.3	
			H_{22}–C_{21}–H_{23}	106.6		C_{10}–C_{12}–C_{21}–H_{23}	59.3	
			H_{22}–C_{21}–H_{24}	108.6		C_{10}–C_{12}–C_{21}–H_{24}	180.0	
			H_{23}–C_{21}–H_{24}	108.6		C_{14}–C_{12}–C_{21}–H_{22}	120.7	
						C_{14}–C_{12}–C_{21}–H_{23}	− 120.7	
						C_{14}–C_{12}–C_{21}–H_{24}	0.0	
						C_{11}–C_{13}–C_{15}–C_{14}	0.0	0.4[a]
						C_{11}–C_{13}–C_{15}–O_{18}	180.0	179.9[a]
						H_{16}–C_{13}–C_{15}–C_{14}	180.0	178.0[a]
						H_{16}–C_{13}–C_{15}–O_{18}	0.0	1.0[a]
						C_{12}–C_{14}–C_{15}–C_{13}	0.0	0.5[a]
						C_{12}–C_{14}–C_{15}–O_{18}	180.0	180.0[a]
						H_{17}–C_{14}–C_{15}–C_{13}	180.0	178.0[a]
						H_{17}–C_{14}–C_{15}–O_{18}	0.0	1.0[a]
						C_{13}–C_{15}–O_{18}–H_{25}	180.0	174.0[a]
						C_{14}–C_{15}–O_{18}–H_{25}	0.0	6.0[a]

[a]Taken from Ref. [Fronczek 2014]

[b]Taken from Ref. [Chotima et al. 2018]

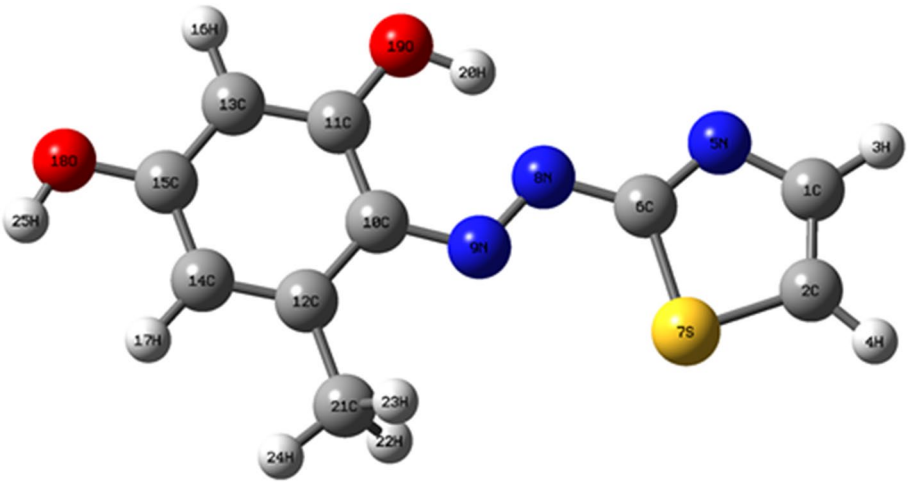


Fig. 3 Molecular structure and atomic numbering of MTR molecule

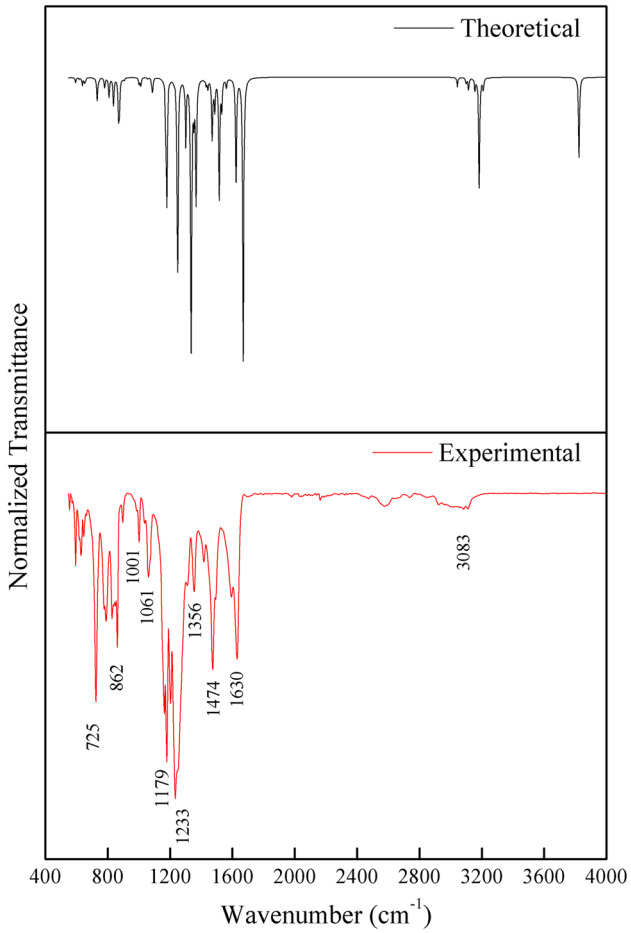


Fig. 4 Theoretical and experimental FT-IR spectra of MTR molecule

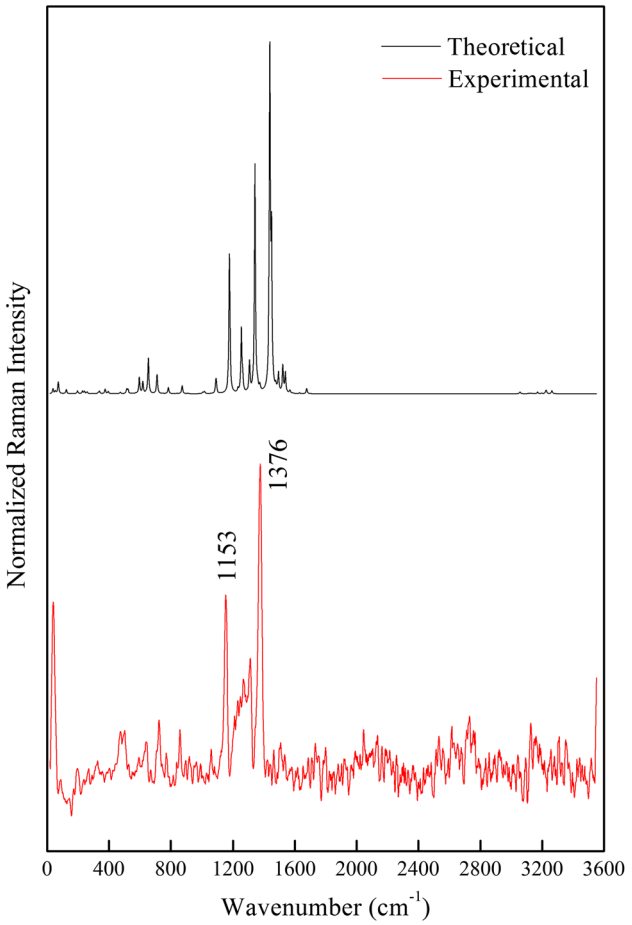


Fig. 5 Theoretical and experimental FT–Raman spectra of MTR molecule

corresponding predicted FT-IR and FT–Raman spectra are given in Figs. 4 and 5. Spectra are shown the observed and predicted wavenumbers, and their relative intensities and total energy distributions of MTR molecule are gathered in Table 2.

The C–H (ν_{CH}) bond-stretching mode was calculated at 3209 and 3249 cm^{-1}, respectively (Varsanyi 1974). In the thizolylazo ring, no these vibrations detected in the experimental process. The predicted peak at 3156, 3184, and 3213 cm^{-1} was assigned to the CH-stretching vibration of

Table 2 Calculated and observed vibrational wavenumbers (cm^{-1}) and potential energy distributions (PED) of MTR

Mode	Symm.	Theoretical			Experimental		PED
		Freq.	I_{IR}	I_{Raman}	FT-IR	FT–Raman	
ν_1	A”	38	0.055	1.037		39 s	$\tau_{CCCH}(25\%)+\tau_{NCCC}(14\%)+\tau_{SCNN}(10\%)+\tau_{CCCC}(10\%)$
ν_2	A”	53	0.141	0.544			$\tau_{NCCC}(20\%)+\tau_{CCCH}(13\%)+\tau_{CCOH}(13\%)+\tau_{NCNN}(11\%)$
ν_4	A”	123	0.204	0.518			$\tau_{CCCH}(69\%)\ CH_3$
ν_5	A”	124	0.002	0.383			$\tau_{CCCH}(64\%)\ CH_3$
ν_6	A”	194	0.131	0.042			$\tau_{CCCH}(35\%)\ CH_3+\tau_{CCCC}(24\%)+\tau_{CCCO}(16\%)\ R_2$
ν_8	A”	228	0.255	0.601			$\tau_{CCCH}(30\%)+\tau_{CCCO}(25\%)+\tau_{CCCH}(15\%)\ R_2$
ν_9	A”	241	0.023	0.526			$\tau_{CCCC}(18\%)+\tau_{CCCH}(17\%)+\tau_{CCCO}(14\%)++\tau_{CCCN}(10\%)\ R_3$
ν_{12}	A”	337	0.360	0.589			$\tau_{NNCN}(25\%)+\tau_{SCNN}(21\%)+\tau_{NCSC}(21\%)\ R_1$-$R_3$
ν_{14}	A”	394	22.13	0.559			$\tau_{CCOH}(66\%)+\tau_{CCCH}(12\%)\ R_2$
ν_{15}	A”	420	0.068	0.049			$\tau_{NCCC}(22\%)+\tau_{CCCH}(20\%)+\tau_{CCCC}(16\%)+\tau_{CCCO}(16\%)$
ν_{19}	A”	541	1.065	0.048	555 m		$\tau_{CSCH}(16\%)+\tau_{CNCH}(46\%)+\tau_{SCCH}(19\%)\ R_1$
ν_{20}	A”	570	0.037	0.076	573 w		$\tau_{CCCH}(39\%)+\tau_{CCCC}(24\%)\ R_3$
ν_{23}	A”	637	2.856	0.150	629 m		$\tau_{NCSC}(11\%)+\tau_{CNCH}(45\%)+\tau_{SCCH}(16\%)\ R_1$
ν_{25}	A”	659	0.873	0.023	662 w		$\tau_{CCCH}(30\%)+\tau_{CCCC}(25\%)+\tau_{CCOH}(11\%)\ R_1$
ν_{27}	A”	733	7.944	0.002	725 s		$\gamma_{NCH}(29\%)+\gamma_{SCH}(30\%)+\tau_{HCCH}(14\%)\ R_1$
ν_{28}	A”	745	0.733	0.043			$\tau_{CCCC}(26\%)+\gamma_{CCH}(23\%)+\tau_{CCCO}(18\%)\ R_2$
ν_{30}	A”	808	6.693	0.046	790 m		$\gamma_{CCH}(43\%)+\gamma_{OCH}\ (19\%)+\tau_{CCCC}(14\%)\ R_2$
ν_{31}	A”	837	9.441	0.083	827 w		$\gamma_{CCH}(40\%)+\gamma_{OCH}(17\%)+\tau_{CCCC}(10\%)\ R_2$
ν_{33}	A”	875	10.37	0.026	862 m		$\gamma_{COH}(60\%)+\tau_{CCCH}(13\%)$
ν_{35}	A”	907	0.795	0.101	993 vw		$\gamma_{CCH}(57\%)+\tau_{HCCS}(18\%)+\tau_{HCNC}(18\%)\ R_1$
ν_{38}	A”	1058	0.491	0.005	1061 m		$\underline{\delta_{HCH}}(57\%)+\tau_{CCCH}(17\%)\ CH_3$
ν_{54}	A”	1478	1.767	0.285	1474 s		$\underline{\delta_{HCH}}(84\%)\ CH_3$
ν_{62}	A”	3100	1.875	0.179	3083 s		$\underline{\nu_{CH}}(76\%)+\tau_{CCCH}(11\%)\ CH_3$
ν_3	A’	72	0.294	2.567			$\tau_{SCNN}(22\%)+\delta_{CNN}(20\%)+\delta_{CCC}(10\%)\ R_1$-$R_3$
ν_7	A’	196	0.915	0.609			$\nu_{OH\ldots N}(30\%)$
ν_{10}	A’	258	0.404	0.415			$\delta_{CC\text{-}CH3}(31\%)+\tau_{NNCC}(15\%)\ R_2$
ν_{11}	A’	328	0.229	0.212			$\delta_{COH}(24\%)+\delta_{CCO}(21\%)+\delta_{CCC}(15\%)\ R_3$
ν_{13}	A’	374	1.416	1.062			$\nu_{OH\ldots N}(30\%)+\delta_{CCO}(20\%)+\delta_{CCC}(13\%)\ R_2$
ν_{16}	A’	471	7.192	0.314			$\nu_{OH\ldots N}(39\%)+\delta_{CCC}(16\%)+\delta_{CCO}(11\%)\ R_3$
ν_{17}	A’	513	2.592	1.047			$\delta_{CCC}(25\%)+\delta_{CCH}(17\%)+\delta_{CCO}(16\%)+\delta_{CSC}(14\%)$
ν_{18}	A’	521	0.745	0.923			$\delta_{CCC}(32\%)+\delta_{CCH}(15\%)+\delta_{CCO}(15\%)+\nu_{CC}(10\%)\ R_3$
ν_{21}	A’	593	1.987	4.004	594 vw		$\nu_{C\text{-}CH3}(15\%)+\delta_{CCC}(23\%)+\tau_{CCCC}(34\%)\ R_2$
ν_{22}	A’	616	0.548	2.850	619 w		$\delta_{CCC}(17\%)+\delta_{CCH}(22\%)\ CH_3+\delta_{CCO}(19\%)\ R_3$
ν_{24}	A’	652	1.725	8.849	647 vw		$\delta_{CCS}(10\%)+\delta_{CSC}(20\%)+\delta_{SCN}(16\%)+\delta_{CCH}(10\%)\ R_1$
ν_{26}	A’	708	0.266	4.839			$\nu_{CS}(43\%)+\delta_{CCH}(25\%)\ R_1$
ν_{29}	A’	780	3.479	1.566	777 w		$\nu_{CS}(20\%)+\nu_{CN}(15\%)+\delta_{CCN}(12\%)+\delta_{CCC}(12\%)+\delta_{NCN}(12\%)\ R_1$
ν_{32}	A’	869	11.94	2.083	851 vw		$\delta_{CCC}(13\%)\ R_1+\nu_{CS}(10\%)+\delta_{SCC}(21\%)\ R_2+\delta_{CNN}(10\%)\ R_3$
ν_{34}	A’	897	0.447	0.046	896 vw		$\delta_{CNC}(29\%)+\delta_{SCC}(12\%)\ R_1+\delta_{CNN}(14\%)\ R_3$
ν_{36}	A’	1001	2.316	0.415	1001 m		$\delta_{HCH}(45\%)+\nu_{C\text{-}CH3}(13\%)\ CH_3+\delta_{CCC}(17\%)\ R_2$
ν_{37}	A’	1012	2.972	0.629	1036 vw		$\delta_{HCH}(39\%)+\nu_{C\text{-}CH3}(17\%)\ CH_3+\delta_{CCH}(14\%)\ R_2$
ν_{39}	A’	1084	2.948	3.236			$\delta_{CCH}(44\%)+\nu_{C\text{-}CH3}(13\%)\ CH_3+\delta_{CCC}(10\%)\ R_2$
ν_{40}	A’	1088	3.029	1.423			$\delta_{CCH}(31\%)+\delta_{HCS}(15\%)\ R_1$
ν_{41}	A’	1172	7.702	38.87	1163vw	1153 s	$\delta_{CCH}(41\%)+\nu_{CN}(16\%)+\delta_{HCN}(10\%)\ R_1$
ν_{42}	A’	1179	42.43	0.489	1179 vs		$\delta_{CCH}(46\%)+\delta_{COH}(29\%)+\nu_{CC}(15\%)\ R_2$
ν_{43}	A’	1226	0.514	1.043	1202 m		$\delta_{CCH}(32\%)+\nu_{CC}(15\%)\ R_2$
ν_{44}	A’	1248	67.00	18.02	1233 vs		$\delta_{COH}(23\%)+\delta_{CCH}(15\%)+\nu_{CN}(13\%)+\nu_{CC}(10\%)$
ν_{45}	A’	1257	2.197	3.759			$\delta_{COH}(21\%)+\delta_{CCH}(19\%)+\nu_{CC}(16\%)+\nu_{CN}(12\%)$
ν_{46}	A’	1301	23.33	8.706	1313 vw		$\nu_{CN}(21\%)\ R_3+\delta_{CCH}(15\%)+\nu_{CC}(20\%)$

Table 2 (continued)

Mode	Symm.	Theoretical			Experimental		PED
		Freq.	I_{IR}	I_{Raman}	FT-IR	FT–Raman	
ν_{47}	A'	1336	97.90	66.45			$\delta_{CCH}(34\%)+\nu_{CC}(11\%)+\delta_{OCH}(12\%)$
ν_{48}	A'	1353	11.38	1.365	1356 m		$\delta_{CCH}(25\%)+\nu_{CC}(15\%)$ R1 $+\delta_{OCH}(18\%)$ R_2
ν_{49}	A'	1367	41.79	1.672		1376 vs	$\nu_{CC}(30\%)+\delta_{CCC}(18\%)+\delta_{CCH}(13\%)+$
ν_{50}	A'	1419	0.333	0.415	1417 w		$\underline{\delta_{HCH}}(70\%)$ CH_3
ν_{51}	A'	1431	2.190	100			$\delta_{CCH}(28\%)+\nu_{CC}(15\%)+\nu_{CN}(13\%)$
ν_{52}	A'	1443	3.272	42.20			$\delta_{CCH}(15\%)+\nu_{CC}(13\%)+\delta_{HCH}(10\%)+\delta_{OCH}(10\%)$
ν_{53}	A'	1470	20.48	1.582			$\nu_{CC}(20\%)+\delta_{CCH}(18\%)+\nu_{CN}(17\%)$
ν_{55}	A'	1487	10.15	5.575	1493 vw		$\underline{\delta_{HCH}}(44\%)$ $CH_3+\delta_{OCH}(10\%)$ R_2
ν_{56}	A'	1515	41.84	8.057			$\delta_{CCH}(53\%)$ $CH_3+\nu_{CC}(13\%)$ R_2
ν_{57}	A'	1532	9.806	6.038			$\delta_{CCH}(30\%)+\nu_{CC}(19\%)+\nu_{CN}(17\%)$
ν_{58}	A'	1561	3.127	0.887	1594 vw		$\nu_{CC}(31\%)+\delta_{CCH}(15\%)$ $R_2+\nu_{CN}(11\%)$ R_3
ν_{59}	A'	1623	37.01	0.273			$\nu_{CC}(38\%)+\delta_{COH}(15\%)+\delta_{CCO}(13\%)$ R_2
ν_{60}	A'	1669	100	1.636	1630 vs		$\nu_{CC}(42\%)+\delta_{CCH}(23\%)$ R_2
ν_{61}	A'	3043	3.263	0.753	3042 m		$\underline{\nu_{CH}}(90\%)$ CH_3
ν_{63}	A'	3115	4.178	0.275			$\underline{\nu_{CH}}(79\%)$ CH_3
ν_{64}	A'	3156	4.169	0.751	3112 w		$\nu_{CH}(72\%)$ R_2
ν_{65}	A'	3184	38.83	0.250			$\nu_{OH}(83\%)$ R_2
ν_{66}	A'	3209	3.448	1.097			$\nu_{CH}(78\%)+\delta(14\%)$ R_1
ν_{67}	A'	3213	0.561	0.790			$\nu_{CH}(69\%)+\delta(11\%)$ R_2
ν_{68}	A'	3249	0.183	1.370			$\nu_{CH}(81\%)$ R_1
ν_{69}	A'	3824	27.68	0.732			$\nu_{OH}(91\%)$

*Experimental frequencies from IR spectrum in cm^{-1}. CH_3 methyl group; R_1 thizolylazo ring; R_2 resorcinol ring; R_3 azo group

**Potential energy distribution calculated at B3LYP/6-311G(d,p) level of theory. Only contributions more than 10% are listed

Vibrational modes: ν stretching; δ in-plane bending; γ out-of-plane bending; τ torsion; *vw* very weak; *w* weak; *m* medium; *s* strong; *vs* very strong

the resorcinol group. One of them could be only measured in the FT-IR spectra. The observed peak at 3112 cm^{-1} was assigned to the CH-stretching vibration of the resorcinol ring in the FT-IR spectra. The symmetric CH-stretching vibrations of the methyl group measured at 3042 cm^{-1} in the FT-IR spectra. This peak predicted at 3043 cm^{-1} with 90% PED contribution by DFT calculation. The asymmetric CH-stretching vibrations were calculated at 3100 and 3115 cm^{-1} by DFT, and detected at 3083 cm^{-1} in the FT-IR spectra. Both thizolylazo ring and resorcinol ring have the two CH-stretching vibrations, which are in-plane vibrations. 3156, 3209, 3213, and 3249 cm^{-1} peak was assigned to the in-plane CH-stretching modes by DFT calculations. One of them was detected by FT-IR spectra. This resorcinol ring was measured at 3112 cm^{-1} by experimental process. Other in-plane CH-stretching vibrations could not be observed any experimental process.

The CH in-plane bending vibrations appear in the region 1400–1050 cm^{-1} and CH out-of-plane bending vibrations in the range of 1000–675 cm^{-1} (Smith 1998; Socrates 2001). In the FT-IR spectra, observations at 1356, 1179, 1202, and 1356 cm^{-1} peak were assigned to the in-plane CH-bending vibrations. Out-of-plane CH-bending vibrations were detected at 993, 827, 790, and 725 cm^{-1} peak in the FT-IR spectra.

The OH group vibrations are the most sensitive to the environment. In the hydrogen-bonded species, the OH group vibrations move the frequencies of the non-hydrogen-bonded species towards to a lower frequency. When hydrogen-bonded species are compared to the non-hydrogen-bonded species, frequencies intensity increased and band broadened. The OH-stretching wave number of the non-hydrogen-bonded or free hydroxyl group appears in the region 3700–3500 cm^{-1} (Michalska et al. 1996), while ones move towards to the 3500–3200 cm^{-1} for hydrogen-bonded formation (Krishnakumar and Muthunatesan 2006). The predicted frequencies of the OH stretching are at 3824 cm^{-1} using DFT calculation with PED contribution of 91%, while no peak observed in the experimental FT-IR spectrum, because of the existence of strong intramolecular hydrogen bonding.

The in-plane OH-bending vibrations are together with in-plane CH-bending and CC-stretching vibrations. In the present work, experimentally observed 1233 cm^{-1} peak has been assigned to OH in-plane bending vibration in IR

spectrum. It shows good agreement with predicted wavenumber at 1248 cm^{-1} (mode no. 44) by DFT calculation with PED contribution of 23%. The OH out-of-plane bending vibrations appear region around 700–600 cm^{-1}. In the present work, out-of-plane OH-bending vibration was measured at 862 cm^{-1} in IR spectrum. This vibration predicted at 875 cm^{-1} by DFT calculation with PED contribution of 60%.

The CH_3 deformation modes are expected in the 1350–1500 cm^{-1} region (Dereli et al. 2012; Sarıkaya et al. 2013; Sundaraganesan et al. 2005). The asymmetric vibration is observed at 1493 cm^{-1}, whereas the symmetric ones were detected at 1474 cm^{-1} in the FT-IR spectra. Other asymmetric CH_3 deformation band could not be observed in the FT-IR spectra. The asymmetric vibrations were calculated at 1515 and 1487 cm^{-1} by DFT. Symmetric ones predicted at 1478 cm^{-1} by DFT. PED contributions were determined at 53, 44, and 84%, respectively. Similarly, vibration mode no: 50 were predicted at 1419 cm^{-1} with 70% PED contribution. The CH_3 rocking modes are usually found at 1010–1070 cm^{-1} (Sundaraganesan et al. 2005). The observed band at 1061 cm^{-1} was assigned to the CH_3 rocking vibration in the FT-IR spectra. This band calculated at 1058 cm^{-1} by means of DFT calculation with 57% PED contribution. In most of the compounds, the asymmetric scissoring appears at a constant range of 1400–1460 cm^{-1} (Wang et al. 2015). The vibrations observed at 1435 and 1417 cm^{-1} in FT-IR and at 1436 and 1412 cm^{-1} in FT Raman are consigned to asymmetrical scissoring vibration and a band observed at 1357 cm^{-1} FT–Raman is assigned to symmetrical scissoring vibration.

The CS-stretching bands are observed in the range of 800 ± 130 cm^{-1} usually with moderate intensity (Roeges 1994). Since the S atom is less electronegative than the O atom, the CS group is not as polar as the CO group and is less prone to form bridges. In the present study, the CS-stretching vibrations is calculated at 708 cm^{-1} with 43% TED and the stretching vibration could not be observed in the FT-IR spectra. The asymmetric CS (ν_{CS}) and symmetric CS (ν_{CS}) bond-stretching mode was calculated at 708 and 780 cm^{-1}, respectively. Furthermore, wavelengths 541, 637, 733, and 907 cm^{-1} were assigned torsion of the thizolylazo ring.

NMR spectra

The nuclear magnetic resonance spectra of the ground-state geometry of MTR molecule have been obtained by the DFT/GIAO method. The NMR spectra calculations were performed for DMSO-d_6 solvent and NMR spectra were measured at room temperature in DMSO-d_6 solvent. Theoretical and experimental ^1H and ^{13}C spectra of the most stable conformer of MTR molecule are given in Table 3 and Fig. 6.

Table 3 The experimental and the theoretical chemical shifts for MTR

	Theoretical	Experimental		Theoretical	Experimental
C_6	185.8				
C_{15}	172.3	175.8	H_3	7.85	7.93
C_{11}	166.3	166.5	H_4	7.44	7.74
C_{12}	155.2	157.8	H_{17}	6.50	6.47
C_1	147.0	144.9	H_{16}	6.38	6.21
C_{10}	138.1	143.5	H_{25}	5.11	3.34
C_2	130.7	130.8	H_{22}	2.87	2.48
C_{14}	115.2	112.4	H_{23}	2.87	2.48
C_{13}	104.9	101.5	H_{24}	2.07	–
C_{21}	22.37	18.11	H_{20}	13.03	13.29

Aromatic carbon gives signals with chemical shift values from 100 to 200 ppm [Subashchandrabose et al. 2010; Joseph et al. 2012; Erdogdu et al. 2009). The observed experimental chemical shift position of ring carbons in MTR lies in the range 172.3–104.9 ppm. The carbon atoms C_{11} and C_{15} are highly de-shielded due to the effect of highly electronegative oxygen attached with these carbon atoms and shows peaks at 172.3 and 166.3 ppm, respectively. The chemical shifts were observed as expected for all the protons. However, ^{13}C NMR chemical shifts were observed some differences when compared with the experimental and theoretical results. The ^{13}C NMR chemical shift of C_{21} is lower than the other carbons due to its methyl group carbon atom.

Chemical shift for protons attached to the thizolylazo ring and resorcinol ring appears in the range at $\delta = 6.21$–7.93 ppm. The chemical shifts of thizolylazo ring ($H_3 = 7.93$ and $H_4 = 7.73$ ppm) are detected higher than those ($H_{16} = 6.21$ ppm and $H_{17} = 6.48$ ppm) of resorcinol ring. The pair of protons H_{22} and H_{23}, which is the two equivalent protons, generates a signal at δ 2.50 ppm. The signal to another proton (H_{24}) of the methyl group was detected at 2.17 ppm. The chemical shifts of H_{22}, H_{23}, and H_{24} were calculated at 2.87 and 2.07 ppm by using DFT calculation. The NMR signals of the H_{20} and H_{25} protons, which are connected oxygen atoms (O_{19} and O_{18}), were measured at 13.29 and 3.34 ppm, respectively. The NMR signal of H_{20} proton was detected higher than this of H_{25} due to hydrogen bonding to the N_8 atom. Predicted at 13.03 ppm chemical shift were to the assignment of H_{20} protons.

UV–Vis spectral analysis

UV–visible spectral analysis of MTR has been performed by the experimental and theoretical methods. The experimental spectrum (Fig. 7) has been observed in the methanol solvent. Absorbance measurement was performed at

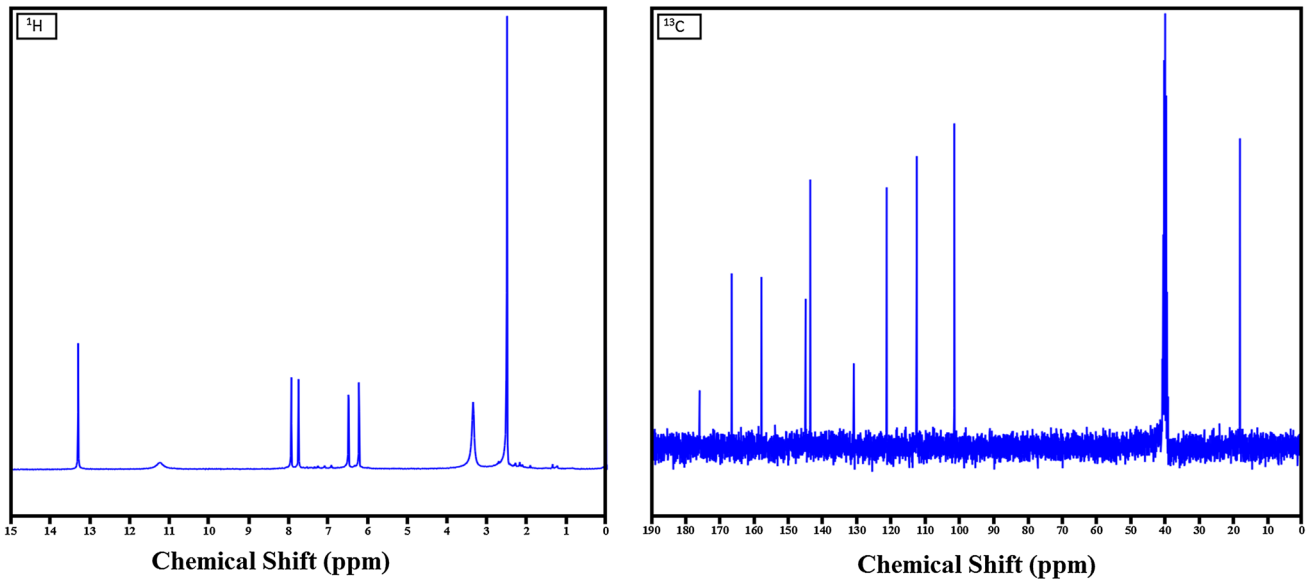


Fig. 6 Experimental NMR spectra of MTR

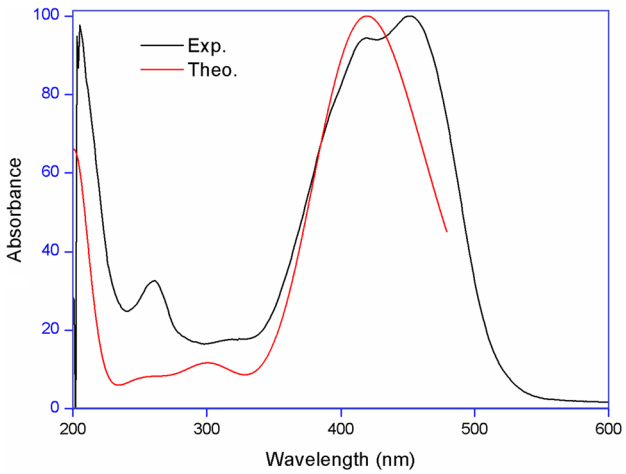


Fig. 7 Theoretical and experimental UV–Vis spectra of MTR molecule

room temperature using 1 cm quartz cuvette in the range of 200–1100 nm. Methanol was used as a blank for the analysis of MTR. Trace amount of MTR was dissolved in methanol to obtain an absorbance spectrum of less than 1.0 absorbance units (a.u.). The optical absorbance spectrum of the MTR is presented in Fig. 6. The combination of the solvent model and the TD-DFT method is required for the computation of the absorption spectra to compare with the experimental results (Table 4). The absorbance maximum was observed in the visible region of the spectrum at 452 nm (0.36 a.u.) and it gives a shoulder at 422 nm (0.34 a.u.). The TD-DFT calculation shows a maximum absorption position at 422 nm with oscillator strength 0.6, which corresponds to HOMO → LUMO transition. The absorbance peaks in ultraviolet region of the spectrum were observed at 262 nm (0.12 a.u.) and 206 nm (0.35 a.u.), respectively.

Electronic properties

To explain the possible charge transfer interaction within the MTR molecule, the highest occupied molecular orbital (HOMO) energy and the lowest unoccupied molecular orbital (LUMO) energy have been computed and the energy gap between them has been calculated. Molecular orbital plots for the ground state of MTR molecule in gas phase including the HOMO-2, HOMO-1, HOMO, LUMO, LUMO+1, and LUMO+2 are shown in Fig. 8. In MTR molecule, HOMO and LUMO are located on the whole molecule without methyl group. LUMO-1 and LUMO-2 are distributed as the LUMO (Subashchandrabose et al. 2012; Fukui 1982; Erdogdu et al. 2014; Gece 2008).

Significant parameter in determining electrical transport properties (Fukui 1982) is frontier orbital energy gap (E_{HOMO}–E_{LUMO}). It is found at 3.222 eV which indicate high excitation energies (in the ultra violet region) and good stability. Frontier orbital energy values such as E_{HOMO-1} = − 6.707 eV; E_{LUMO+1} = − 0.373 eV; E_{HOMO-2} = − 6.925 eV; E_{LUMO+2} = − 0.249 eV is also calculated. In addition, the electron affinity (A), ionization potential (I), global hardness (η), softness (S), chemical potential (μ), electronegativity (χ), and electrophilicity can be calculated by means of HOMO and LUMO energy values. In the gas phase of the MTR molecule, A and I were computed at 2.843 eV and 6.065 eV, respectively. Global hardness (η), softness (S), chemical potential (μ), electronegativity (χ),

Table 4 Computation of the absorption spectra to compare with the experimental results of MTR

	Exp. wavelength (nm)	Energy (eV)	Cal. wavelength (nm)	Osc. strength	Symmetry	Major contributes
1	453	2.932	422.8	0.6941	Singlet-A'	HOMO → LUMO (69%)
2		3.199	387.4	0.1044	Singlet-A'	H-1 → LUMO (68%)
3	260	4.092	302.9	0.0831	Singlet-A'	H-3 → LUMO (67%)
4		4.195	295.5	0.0001	Singlet-A"	H-4 → LUMO (70%)
5		4.686	264.5	0.0424	Singlet-A'	H-5 → LUMO (68%)
6		5.108	242.7	0.0359	Singlet-A'	HOMO → L+1 (48%); HOMO → L+2(41%)
7		5.420	228.7	0.0025	Singlet-A'	HOMO → L+1 (36); HOMO → L+2(42)
8		5.556	223.1	0.0001	Singlet-A"	HOMO → L+3(68)
9		5.926	209.2	0.0772	Singlet-A'	H-1 → L+1 (62)
10	206	6.124	202.4	0.2616	Singlet-A'	H-1 → L+2 (50); HOMO → L+4(41)

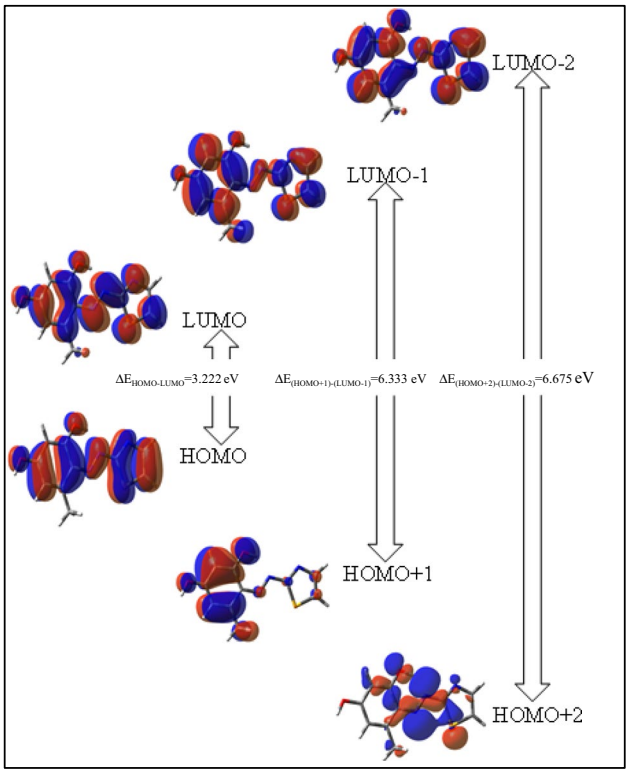


Fig. 8 HOMO–LUMO plots of MTR molecule

and electrophilicity were calculated 1.611 eV, 0.620 $(eV)^{-1}$, −4.454 eV, 4.454 eV, and 6.157 eV, respectively (Table 5).

Molecular electrostatic potential (MEP)

Electrostatic potential maps are very useful three-dimensional diagram for the investigation of the molecular structure with its physiochemical property relationships (Luque et al. 2000; Okulik and Jubert 2005; Parlak et al. 2011). The molecular electrostatic potential diagrams used

Table 5 Calculated some properties values of MTR in its ground state [B3LYP/6-311G(d,p)]

E_{HOMO} (eV)	− 6.065	Ionization potential (I) (eV)	6.065
E_{LUMO} (eV)	− 2.843	Electron affinity (A) (eV)	2.843
E_{H-L} gap (eV)	3.222	Global hardness (η)(eV)	1.611
E_{HOMO-1} (eV)	− 6.707	Softness (S) $(eV)^{-1}$	0.620
E_{LUMO+1} (eV)	− 0.373	Chemical potential (μ)(eV)	− 4.454
$E_{(H-1)-(L+1)}$ gap (eV)	6.333	Electronegativity (χ)(eV)	4.454
E_{HOMO-2} (eV)	− 6.925	Electrophilicity (eV)	6.157
E_{LUMO+2} (eV)	− 0.249		
$E_{(H-2)-(L+2)}$ gap (eV)	6.675		

to visualize the charge distributions and charge-related properties. Total electron density and molecular electrostatic potential plot of MTR molecule predicted by DFT [B3LYP/6-311G(d,p)] method are given in Fig. 9 for MTR molecule. In the color scheme for the MEP surface, red-color region is electron rich or partially negative charge. Blue color region has the electron-deficient or partially positive charge. Light blue region has slightly electron-deficient region. Yellow color region has slightly electron-rich region. In the MEP of MTR molecule, oxygen atoms are the electron-rich centers.

Density of state (DOS)

The DOS is predicted and formed using the Gauss-Sum2.2 software. The information of molecular orbital is transformed using the Gaussian curves of unit height and full width at half maximum (FWHM) of 0.3 eV. In the present work, the DOS plot of MTR is shown in Fig. 10. It provides a pictorial representation of molecule orbital compositions and their contributions to chemical bonding (Asath et al. 2017; Boyle et al. 2008).

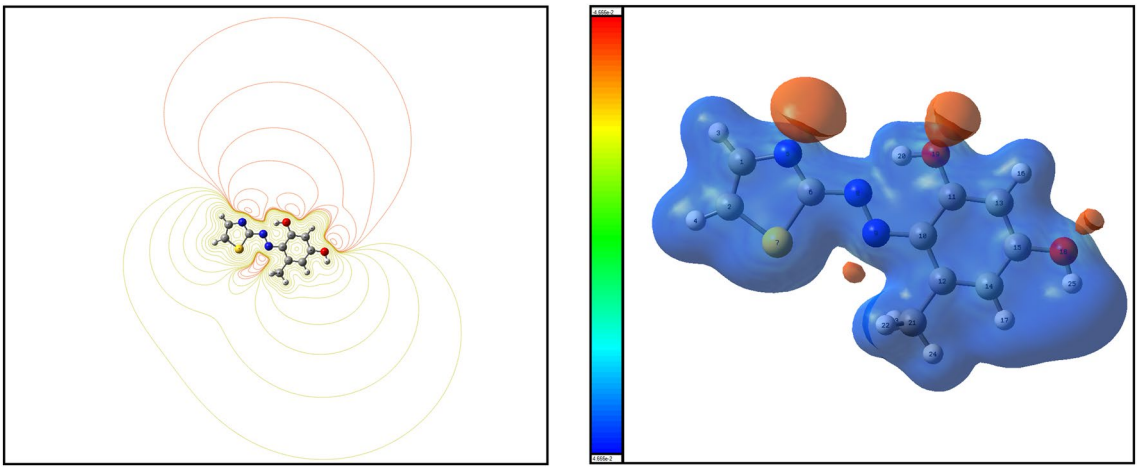


Fig. 9 Total electron density and molecular electrostatic potential plot of MTR molecule

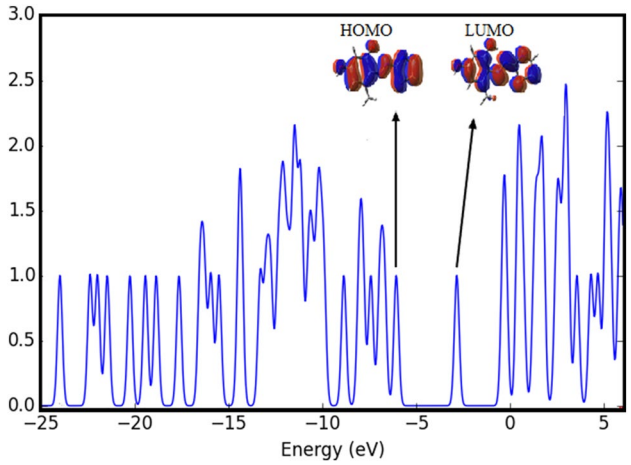


Fig. 10 Density-of-state plot of MTR molecule

Table 6 The electric dipole moment μ (Debye), average polarizability $\bar{\alpha}$, anisotropy of polarizability $\Delta\alpha$ (10^{-24} *esu*), and first hyperpolarizability $_0$ (10^{-30} *esu*) of the title molecule

μ_x	− 3.621	β_{xxx}	− 0.77	μ	4.396
μ_y	2.052	β_{xyy}	2.499	α	28.859
μ_z	0	β_{xzz}	0	Δα	37.664
		β_{yyy}	3.529	β_x	1.729
α_{xx}	39.516	β_{xxy}	2.755	β_y	6.537
α_{xy}	14.32	β_{yzz}	0.253	β_z	− 0.05
α_{yy}	37.044	β_{zzz}	0		
α_{xz}	0	β_{yyz}	0	β_{tot}	6.762
α_{yz}	0	β_{xxz}	− 0.05		
α_{zz}	10.017	β_{yxz}	0		

Non-linear optical (NLO) properties

In the present work, non-linear optical properties (dipole moment, polarizability, and first-order hyperpolarizability) of MTR molecule were determined by mean of DFT [B3LYP/6-311G(d, p)] approximation. The computed NLO properties are listed in Table 6. Some selected NLO properties, which are static dipole moment (μ), the mean polarizability ($\bar{\alpha}$), the anisotropy of the polarizability ($\Delta\alpha$), and the mean first-order hyperpolarizability (β_0), are described as follows (Kleinman 1962; Zhang et al. 2010):

$$\mu^2 = \mu_x^2 + \mu_y^2 + \mu_z^2 \tag{1}$$

$$\bar{\alpha} = \left(\alpha_{xx} + \alpha_{yy} + \alpha_{zz}\right)/3 \tag{2}$$

$$\Delta\alpha = \frac{1}{\sqrt{2}}\left[\left(\alpha_{xx} - \alpha_{yy}\right)^2 + \left(\alpha_{yy} - \alpha_{zz}\right)^2 + \left(\alpha_{zz} - \alpha_{xx}\right)^2 + 6(\alpha_{xy}^2 + \alpha_{yz}^2 + \alpha_{xz}^2)\right]^{1/2} \tag{3}$$

$$\beta_0 = \left[\left(\beta_{xxx} + \beta_{xyy} + \beta_{xzz}\right)^2 + \left(\beta_{yyy} + \beta_{xxy} + \beta_{yzz}\right)^2 + \left(\beta_{zzz} + \beta_{xxz} + \beta_{yyz}\right)^2\right]^{1/2}. \tag{4}$$

Great value of a specific component of the polarizability and hyperpolarizability points out a substation delocalization of charge (Karamanis et al. 2008). Theoretically, the first hyperpolarizability of the MTR is 17.85 times higher than ones of urea (β_0 of urea is 0.3728×10^{-30} *esu*). Thus, MTR exhibited good NLO activity. Therefore, the title molecule is proposed to the potential applications in the development of non-linear optical materials (Velraj et al. 2015).

Conclusions

The experimental (FT-IR, FT–Raman, NMR, and UV–Vis spectra) and conformational analysis, theoretical wave number and their intensity, total energy distributions, some electronic properties such as E_{HOMO}, E_{LUMO}, electron affinity, ionization potential, global hardness, softness, chemical potential, electronegativity, and electrophilicity of MTR molecule have been determined.

- The free MTR molecule has eight conformers. According to the lowest energy conformer, the relative energy of the higher energy conformers was obtained at 3.806 kcal/mol, 4.236 kcal/mol, and 7.345 kcal/mol, respectively. The result of conformational analysis shows that conformer-1 is favorable than the other conformers at room temperature.
- The MTR molecule possesses C_s point group symmetry and has 25 atoms ($C_{10}H_9N_3O_2S$) with 69 normal modes. All the vibrations are active in both IR and Raman spectra. The calculated frequencies are in good agreement with the experimental ones.
- The Nuclear Magnetic Resonance spectra of the ground-state geometry of MTR molecule have been obtained by the DFT/GIAO method. The TD-DFT calculation shows a maximum absorption position at 422 nm with an oscillator strength 0.6, which corresponds to HOMO → LUMO transition. The absorbance peaks in ultraviolet region of the spectrum were observed at 262 nm (0.12 a.u.) and 206 nm (0.35 a.u.), respectively.

References

Asath RM, Premkumar S, Mathavan T, Benial AMF (2017) Vibrational spectroscopic, molecular docking and quantum chemical studies on 6-aminonicotinamide. J Mol Struct 1134:143–156. https://doi.org/10.1016/j.molstruc.2016.12.058

Becke AD (1988) Density-functional exchange-energy approximation with correct asymptotic behavior. Phys Rev A 38:3098–3100. https://doi.org/10.1103/PhysRevA.38.3098

Becke AD (1993) Density-functional thermochemistry. III. The role of exact exchange. J Chem Phys 98:5648–5652. https://doi.org/10.1063/1.464913

Boyle NMO, Tenderholt AL, Langner KM (2008) Cclib: a library for package-independent computational chemistry algorithms. J Comput Chem 29:839–845. https://doi.org/10.1002/jcc.20823

Brockway LO, Roberts JM (1939) The crystal structure of hexamethylbenzene and the length of the methyl group bond to aromatic carbon atoms. J Chem Soc. https://doi.org/10.1039/jr9390001324

Chotima R, Boonseng B, Piyasaengthong A, Songsasen A, Chainok K (2018) Crystal structure of 3-[2-(1,3-thia-zol-2-yl)diazen-1-yl] pyridine-2,6-di-amine monohydrate. Acta Cryst E74:563–565

Chung Y, Chung W (2003) Determination of Co(II) Ion as 4-(2-thiazolylazo) resorcinol or 5-methyl-4-(2-thiazolylazo)resorcinol chelate by reversed-phase capillary high-performance liquid chromatography. Bull Korean Chem Soc 24(12):1781–1784. https://doi.org/10.5012/bkcs.2003.24.12.1781

Dereli Ö, Erdogdu Y, Gulluoglu MT, Türkkan E, Özmen A, Sundaraganesan N (2012) Vibrational spectral and quantum chemical investigations of tert-butyl-hydroquinone. J Mol Struct 1012:168–176. https://doi.org/10.1016/j.molstruc.2012.01.003

Erdogdu Y, Güllüoğlu MT, Kurt M (2009) DFT, FT-Raman, FT-IR and NMR studies of 2-fluorophenylboronic acid. J Raman Spect 40(11):1615–1623. https://doi.org/10.1002/jrs.2309

Erdogdu Y, Guzel M, Güllüoglu MT, Amalanathan M, Saglam S, Joe IH (2014) Molecular structure, vibrational spectral investigation and the conformational analysis of 4-methylesculetin. Opt Spectrosc 116:348–359. https://doi.org/10.1134/s0030400x14030059

Frisch A, Nielson AB, Holder AJ (2000) Gaussview user manual. Gaussian Inc., Pittsburgh

Frisch MJ et al (2009) Gaussian 09 Revision B.01. Gaussian Inc., Wallingford

Fronczek FR (2014) Experimental crystal structure determination, Deposition code CCDC 168981. https://doi.org/10.5517/cc5nv0n

Fukui K (1982) Role of frontier orbitals in chemical reactions. Science 218:747–754. https://doi.org/10.1126/science.218.4574.747

Gaokar UG, Eshwar MC (1982) Rapid spectrophotometric determination of manganese(II) with 4-(2-thiazolylazo)-resorcinol. Mikrochim Acta 78:247–252. https://doi.org/10.1007/BF01206924

Gavazov KB, Lekova VD, Dimitrov AN, Patronov GI (2007) The solvent extraction and spectrophotometric determination of vanadium (V) with 4-(2-thiazolylazo)resorcinol and tetrazolium salts. Cent Eur J Chem 5(1):257–270. https://doi.org/10.2478/s11532-006-0053-x

Gece G (2008) The use of quantum chemical methods in corrosion inhibitor studies. Corros Sci 50:2981–2992. https://doi.org/10.1016/j.corsci.2008.08.043

Halgren TA (1996) Merck molecular force field. I. Basis, form, scope, parameterization, and performance of MMFF94J. Comput Chem 17:490–519. https://doi.org/10.1002/(SICI)1096-987X(199604)17:5/6%3c490:AID-JCC1%3e3.0.CO;2-P

Joseph L, Sajan D, Reshmy R, Sasi BSA, Erdogdu Y, Thomas KK (2012) Vibrational spectra, structural conformations, scaled quantum chemical calculations and NBO analysis of 3-acetyl-7-methoxycoumarinSpectrochim. Acta Part A 99:234–247. https://doi.org/10.1016/j.saa.2012.07.084

Karamanis P, Pouchan C, Maroulis G (2008) Structure, stability, dipole polarizability and differential polarizability in small gallium arsenide clusters from all-electron ab initio and density-functional-theory calculations. Phys Rev A 77:013201. https://doi.org/10.1103/physreva.77.013201

Kleinman DA (1962) Nonlinear Dielectric polarization in optical media. Phys Rev 126:1977–1979. https://doi.org/10.1103/PhysRev.126.1977

Krishnakumar V, Muthunatesan S (2006) FT-IR, FT-Raman spectra and scaled quantum mechanical study of 2,3-dihydroxy pyridine and 2,4-dihyroxy-3-nitropyridine. Spectrochim Acta A 65:818–825. https://doi.org/10.1016/j.saa.2005.12.039

Lee C, Yang W, Parr RG (1988) Development of the Colle-Salvetti correlation-energy formula into a functional of the electron density. Phys Rev B37:785–789. https://doi.org/10.1103/PhysRevB.37.785

Luque FJ, Lopez JM, Orozco M (2000) Perspective on "Electrostatic interactions of a solute with a continuum. A direct utilization of ab initio molecular potentials for the prevision of solvent effects. Theor Chem Acc 103:343–345. https://doi.org/10.1007/s002149900013

Menek N, Eren E, Topcu S (2006) Kinetic investigation of an azo dye oxidation by hydrogen peroxide in aqueous surfactant solution. Dyes Pigment 68:205–210. https://doi.org/10.1016/j.dyepig.2005.01.010

Michalska D (2003) RAINT program. Wroclaw University of Technology, Poland
Michalska D, Bienko DC, Bienko AJA, Latajaka Z (1996) Density functional, Hartree—Fock, and MP2 studies on the vibrational spectrum of phenol. J Phys Chem 100:17786–17790. https://doi.org/10.1021/jp961376v
Okulik N, Jubert AH (2005) Theoretical analysis of the reactive sites of non–steroidal anti–inflammatory drugs. J Mol Des 4:17–30. http://www.biochempress.com. Accessed 1 Sept 2019
Parlak C, Akdogan M, Yildirim G, Karagoz N, Budak E, Terzioglu C (2011) Density functional theory study on the identification of 3-[(2-morpholinoethylimino)methyl]benzene-1,2-diol. Spectrochim Acta Part A 79:263–271. https://doi.org/10.1016/j.saa.2011.02.057
Robertson JM (1936) The structure of resorcinol a quantitative X-ray investigation. Proc R Soc A Math Phys Sci 157(890):79–99. https://doi.org/10.1098/rspa.1936.0181
Roeges NPG (1994) A guide to the complete interpretation of infrared spectral od organic structures. Wiley, New York
Sarıkaya EK, Dereli Ö, Erdogdu Y, Güllüoglu MT (2013) Molecular structure and vibrational spectra of 7-ethoxycoumarin by density functional method. J Mol Struct 1049:220–226. https://doi.org/10.1016/j.molstruc.2013.06.026
Schlegel HB (1975). PhD thesis, Queen's University, Kingston, Ontario, Canada
Seferoğlu Z, Ertan N, Kickelbick G, Hökelek T (2009) Single crystal X-ray structure analysis for two thiazolylazo indole dyes. Dyes Pigm 82:20–25. https://doi.org/10.1016/j.dyepig.2008.10.020
Smith BC (1998) Infrared spectral interpretation: a systematic approach. CRC Press, Boca Raton
Smolinska M, Korkuna O, Vrublevska T, Rudchuk P, Teslyar G (2015) Development and validation of the simple and sensitive spectrophotometric method of sulphanilamides determination with 4-(2-thiazolylazo)-resorcinol in veterinary preparations. Open Chem 13:1254–1268. https://doi.org/10.1515/chem-2015-0139
Socrates G (2001) Infrared and Raman characteristic group frequencies—tables and charts, 3rd edn. Wiley, Chichester
Soylak M, Tuzen M (2008) Coprecipitation of gold(III), palladium(II) and lead(II) for their flame atomic absorption spectrometric determinations. J Hazard Mater 152:656–661. https://doi.org/10.1016/j.jhazmat.2007.07.027
Spartan 18 (2008), Wavefunction, Irvine, CA, USA
SQM version 1.0, Scaled Quantum Mechanical Force Field (2013) Green acres road. Fayetteville, Arkansas, p 72703
Subashchandrabose S, Krishnan AR, Saleem H, Thanikachalam V, Manikandan G, Erdogdu Y (2010) FT-IR, FT-Raman, NMR spectral analysis and theoretical NBO, HOMO–LUMO analysis of bis(4-amino-5-mercapto-1,2,4-triazol-3-yl)ethane by ab initio HF and DFT methods. J Mol Struct 981:59–70. https://doi.org/10.1016/j.molstruc.2010.07.025
Subashchandrabose S, Saleem H, Erdogdu Y, Dereli Ö, Thanikachalam V, Jayabharathi J (2012) Structural, vibrational and hyperpolarizability calculation of (*E*)-2-(2-hydroxybenzylideneamino)-3-methylbutanoic acid. Spectrochim Acta Part A 86:231–241. https://doi.org/10.1016/j.saa.2011.10.029
Subrahmanyam B, Eshwar MC (1976a) Rapid extraction-spectrophotometric determination of gold(III) with 4-(2-thiazolylazo)-resorcinol. Anal Chim Acta 82:435–437. https://doi.org/10.1016/S0003-2670(01)84623-7
Subrahmanyam B, Eshwar MC (1976b) Spectrophotometric determination of chromium(III) with 4-(2-thiazolylazo)-resorcinol. Mikrochim Acta 66:579–584. https://doi.org/10.1007/BF01220116
Sundaraganesan N, Saleem H, Mohan S, Ramalingam M, Sethuraman V (2005) FTIR, FT-Raman spectra and ab initio DFT vibrational analysis of 2-bromo-4-methyl-phenylamine, Spectrochim. Acta A 62:740–751. https://doi.org/10.1016/j.saa.2005.02.043
Varsanyi G (1974) Assignments for vibrational spectra of seven hundred benzene derivatives, vol I. Adam Hilger, London
Velraj G, Soundharam S, Sridevi C (2015) Investigation of structure, vibrational, electronic, NBO and NMR analyses of 2-chloro-4-nitropyridine (CNP), 2-chloro-4-methyl-5-nitropyridine (CMNP) and 3-amino-2-chloro-4-methylpyridine (ACMP) by experimental and theoretical approach. Spectrochimica Acta Part A 137:790–803. https://doi.org/10.1016/j.saa.2014.08.075
Wang Z, Chen J, Li L, Zhou Z, Geng Y, Sun T (2015) Detailed structural study of β-artemether: density functional theory (DFT) calculations of Infrared, Raman spectroscopy, and vibrational circular dichroism. J Mol Struct 1097:61–68. https://doi.org/10.1016/j.molstruc.2015.04.039
Zaitoun MA, El-Qisairi AK, Momani KA, Qaseer HA, Alhalasah W (2014a) Solid-phase extraction employing 5-methyl-4-(2-thiazolylazo)resorcinol entrapped in sol-gel glass as a sorbent resin to remove Zinc ions. J Environ Occup Sci 3:154–161. https://doi.org/10.5455/jeos.20140909071020
Zaitoun MA, Momani K, Jaradat Q, Momani I, Qurashi I (2014b) Synthesis of an organic chelate doped sol gel filter to remove Cu(II) ions from aqueous solutions. Jordan J Chem 9(2):81–96. https://doi.org/10.12816/0026472
Zhang R, Dub B, Sun G, Sun Y (2010) Experimental and theoretical studies on o-, m- and p-chlorobenzylidene aminoantipyrines. Spectrochim Acta Part A 75:1115–1124. https://doi.org/10.1016/j.saa.2009.12.067

Publisher's Note Springer Nature remains neutral with regard to jurisdictional claims in published maps and institutional affiliations.